Check for updates

View Article Online
View Journal

Sustainable Energy & Fuels

Interdisciplinary research for the development of sustainable energy technologies

Accepted Manuscript

This article can be cited before page numbers have been issued, to do this please use: J. Y. Kim, Y. C. Kim and D. K. Moon, *Sustainable Energy Fuels*, 2026, DOI: 10.1039/D5SE01315A.

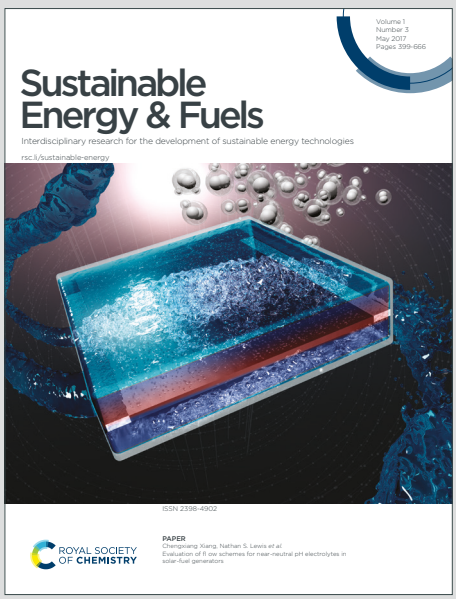

This is an Accepted Manuscript, which has been through the Royal Society of Chemistry peer review process and has been accepted for publication.

Accepted Manuscripts are published online shortly after acceptance, before technical editing, formatting and proof reading. Using this free service, authors can make their results available to the community, in citable form, before we publish the edited article. We will replace this Accepted Manuscript with the edited and formatted Advance Article as soon as it is available.

You can find more information about Accepted Manuscripts in the Information for Authors.

Please note that technical editing may introduce minor changes to the text and/or graphics, which may alter content. The journal's standard Terms & Conditions and the Ethical guidelines still apply. In no event shall the Royal Society of Chemistry be held responsible for any errors or omissions in this Accepted Manuscript or any consequences arising from the use of any information it contains.

ROYAL SOCIETY OF CHEMISTRY

rsc.li/sustainable-energy

View Article Online
DOI: 10.1039/D5SE01315A

ARCLE

Received 00th January 20xx,

Accepted 00th January 20xx

DOI: 10.1039/x0xx00000x

Stability-Oriented Design of MoO_3/TAPC Hybrid Bilayer Hole Transport Layer for Scalable Organic Solar Cells

Ji Youn Kim, Ye Chan Kim, and Doo Kyung Moon*

Organic solar cells (OSCs), recognized for their scalability, lightweight, mechanical flexibility, and solution processability, increasingly empoly interfacial engineering strategies to boost device performance, enhance scalability, and lower overall costs. Herein, we introduce a hybrid bilayer hole transport layer (HTL) strategy that integrates TAPC (4,4′-cyclohexylidenebis[*N*,*N*-bis(4-methylphenyl)benzenamine]) with MoO_3 to simultaneously address the stability limitations of conventional MoO_3 and enhance the scalability of inverted OSCs. Spin-coated TAPC interlayer beneath a thermally evaporated MoO_3 layer suppresses interfacial recombination and facilitates charge transport through its well-aligned energy levels and optimized surface morphology. The hybrid HTL, consisting of a 2.5 nm MoO_3 layer on 0.5 mg mL^{-1} TAPC, delivers reliable long-term operational photostability while retaining device efficiency, achieving a power conversion efficiency (PCE) of 16.49% in unit cells without compromising device performance compared to the single-layer MoO_3. Futhemore, when scaled up to a mini-module (4.725 cm^2), the same device architecture maintained achieved a PCE of 13.95%. These results demonstrate the potential of MoO_3/TAPC hybrid HTLs as a scalable and stable architecture, enabled by their favorable electrical properties and efficient interface engineering.

Introduction

Organic solar cells (OSCs) have garnered considerable attention due to their advantages, including lightweight, semitransparency, low-cost solution process, and compatibility with large-area production.[1–3] Recent advancements in polymer donors and non-fullerene acceptors (NFAs) have effectively improved device performance, pushing the power conversion efficiency (PCE) of OSCs beyond 20%.[4–7] Interfacial layers such as hole transport layers (HTLs) and electron transport layers (ETLs) are indispensable for achieving such progress, as they facilitate selective charge extraction and suppress interfacial recombination.[8,9] Among the available HTLs, molybdenum trioxide (MoO_3) has emerged as a leading alternative to the conventional PEDOT:PSS, offering favorable work function alignment and excellent ambient stability.[10,11] However, MoO_3 exhibits intrinsic instability under illumination, primarily due to photo-induced reduction that lowers its work function.[12,13] In addition, thermally induced degradation accelerates interfacial deterioration during device operation, leading to severe performance loss.[14] These issues significantly limit the long-term operational stability of OSCs employing MoO_3 as a single HTL layer. To address this, Xi *et al*. reported that thermal annealing triggers MoO_3 diffusion and interfacial reactions, which cause substantial efficiency decay, and that introducing a thin 4,4′,4″-tris(carbazol-9-yl)-triphenylamine (TCTA) interlayer can effectively mitigate these degradation pathways. As a result, in long-term thermal stability tests performed at 85°C under encapsulation for 1000 h, the control device retained only 76% of its initial efficiency (17.06% → 13.04%), whereas the TCTA-based device preserved 91% of its initial value (15.92% → 14.45%), demonstrating markedly improved operational durability.[15] Additionally, various interfacial engineering strategies, including bilayer HTLs and molecular doping, have been proposed to address the limitations of MoO_3.[11] Zheng *et al*. systematically compared PM6:BTP-eC9-based OSCs employing different interfacial architectures, including a single self-assembled monolayer (SAMs), a single MoO_3 layer, and a MoO_3/SAM bilayer structure on ITO substrates. This bilayer configuration demonstrated superior performance, achieving a PCE of 19.9%, compared to 18.4% for single MoO_3 and 19.0% for single SAM, primarily due to enhanced charge transport and suppressed interfacial recombination.[7] Previous studies have also shown that introducing a hybrid HTL (*h*-HTL) can improve device efficiency from 9.2% to 12.2%, as demonstrated by doping a small amount of MoO_3 into PEDOT:PSS, which enhances electrical conductivity, energy-level alignment, and interfacial properties.[16]

4,4′-cyclohexylidenebis[*N*,*N*-bis(4-methylphenyl)benzenamine] (TAPC) has been widely utilized in the field of Organic Light-Emitting Diodes (OLEDs) due to its excellent hole mobility and optical transparency, and its potential applicability has recently been reported in emerging photovoltaic architectures.[17] Due to its wide bandgap and low absorption in the visible region, TAPC is considered a suitable donor material for semi-transparent OSCs (ST-OSCs).

[a] Department of Chemical Engineering Konkuk University, Seoul 05029, Republic of Korea. E-mail : dkmoon@konkuk.ac.kr

†Electronic Supplementary Information (ESI) available.

Published on 05 February 2026. Downloaded on 2/27/2026 1:10:22 AM.

Sustainable Energy & Fuels Accepted Manuscript

View Article Online
DOI: 10.1039/D5SE01315A

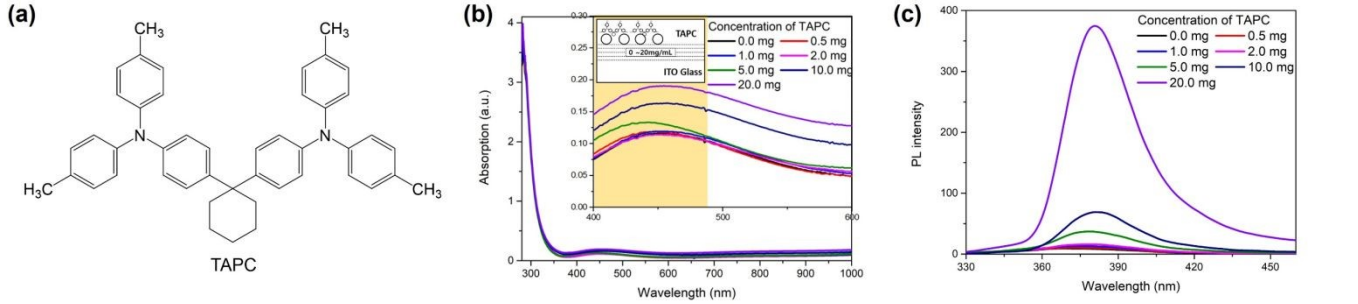

Fig. 1 (a) Chemical structures of TAPC. (b) Normalized absorption spectra of ITO/TAPC films with different TAPC concentrations using methanol. (c) PL spectra of ITO/TAPC films with different TAPC concentrations.

Tang *et al*. fabricated inverted ST-OSCs based on a TAPC:Y6 blend, achieving an enhanced PCE from 2.13% to 3.01%, along with an increase in the average visible transmittance (AVT) from 44.85% to 47.99%.[18] However, the direct application of TAPC in highly efficient OSCs is constrained by its poor oxidative stability and limited interfacial compatibility.[19] Its potential could be further exploited by integrating it with inorganic oxides such as MoO_3 in a hybrid HTL structure, which is anticipated to provide complementary advantages in efficiency and stability.

In this study, we present a hybrid HTL strategy that integrates TAPC and MoO_3 in a bilayer configuration. Introducing a thin TAPC interlayer beneath MoO_3 enhances hole extraction, suppresses interfacial recombination, and improves interfacial morphology, thereby enabling stable device performance without sacrificing efficiency. When applied to PM6:L8-BO - based inverted OSCs, the MoO_3/TAPC hybrid HTL achieved a PCE of 16.49%, comparable to 16.39% for the single-layer MoO_3 device. This parity in efficiency can be attributed to the granular morphology of TAPC, which improves interfacial contact with the active layer and facilitates charge transport. Importantly, the hybrid devices exhibited superior long-term operational stability, retaining performance under continuous 1-sun illumination for 350 h, whereas the MoO_3-only cells degraded more rapidly. Enhanced stability is ascribed to the TAPC, which suppresses interfacial charge recombination. Furthermore, in OSC modules, the MoO_3/TAPC hybrid HTL yielded a PCE of 13.95%, a value comparable to the 13.46% of single-layer MoO_3, confirming the scalability of this strategy. Taken together, our findings demonstrate that the MoO_3/TAPC hybrid HTL enables stable and scalable OSCs without efficiency loss, representing a promising step toward the commercialization of high-performance OSCs.

Results and discussion

Fig. 1a illustrates the chemical structure of TAPC, a conjugated small molecule widely recognized as a wide-bandgap material.[18,20] Fig. S1 shows the UV–Vis spectra of TAPC dispersed in methanol and uniformly distributed by ultrasonication. Across the UV–Vis spectra of TAPC dispersions prepared at concentrations of 0.5, 1, 2, 5, 10, and 20 mg/mL, the maximum absorption wavelength (λ_{max}) was uniformly observed at 282 nm. Moreover, the absorbance was observed to increase proportionally with increasing TAPC concentration. Consistent with previous reports,[18] the optical bandgap of the TAPC film was calculated to be 4.40 eV. As this extends beyond the conventional absorption window of the active layer, TAPC avoids impeding light harvesting and rather functions as efficient charge transport.[21] Fig. 1b presents the UV–Vis spectra of the film fabricated by spin-coating a TAPC dispersion. Unlike the measurements obtained in the dispersion state, the films exhibited nearly identical absorption behavior at λ_{max} = 282 nm regardless of concentration, while displaying a slight increase in intensity within the 400–1000 nm range as the concentration increased. Notably, a broad absorption feature appeared in the 400–600 nm region, with its intensity progressively enhanced as the concentration increased. Such enhancement may be attributed to variations in the optical path of incident light, which influence the apparent absorption behavior due to scattering interactions with the ITO substrate.[22] Fig. 1c displays the photoluminescence (PL) spectra obtained from the TAPC thin film coated onto ITO glass. For the TAPC sample, emission was observed in the range of 380–420 nm, and the PL intensity became stronger as concentration increased. In particular, the TAPC film coated at a concentration of 20 mg/mL exhibited a markedly enhanced peak compared to the 0 mg/mL sample. Collectively, these findings imply that TAPC not only improves light absorption but also strengthens light-extraction capability, which in turn supports better device performance in OSCs.[23,24]

To investigate the MoO_3/TAPC hybrid HTL, we fabricated inverted-structure devices with the configuration ITO/ZnO/PM6:L8-BO/HTL/Ag. The HTL was prepared either as a single-layer MoO_3 or as a MoO_3/TAPC hybrid bilayer, where TAPC was first deposited by spin coating followed by MoO_3 deposition through thermal evaporation. To determine the optimal conditions for the MoO_3 thickness and TAPC concentration, the MoO_3 layer was varied from 0 to 10 nm, and summarized in Fig. S2 and Table S1. The PCE, which was a mere 0.97% at a MoO_3 thickness of 0 nm, exhibited a dramatic surge to a peak value of 16.39% at 2.5 nm, representing the optimal device performance. However, as the thickness further increased, the PCE gradually declined to 15.71% at 5 nm and 11.94% at 10 nm, with a substantial performance degradation observed at the 10 nm mark.

Published on 05 February 2026. Downloaded on 2/27/2026 1:10:22 AM.

Sustainable Energy & Fuels Accepted Manuscript

View Article Online
DOI: 10.1039/D5SE01315A

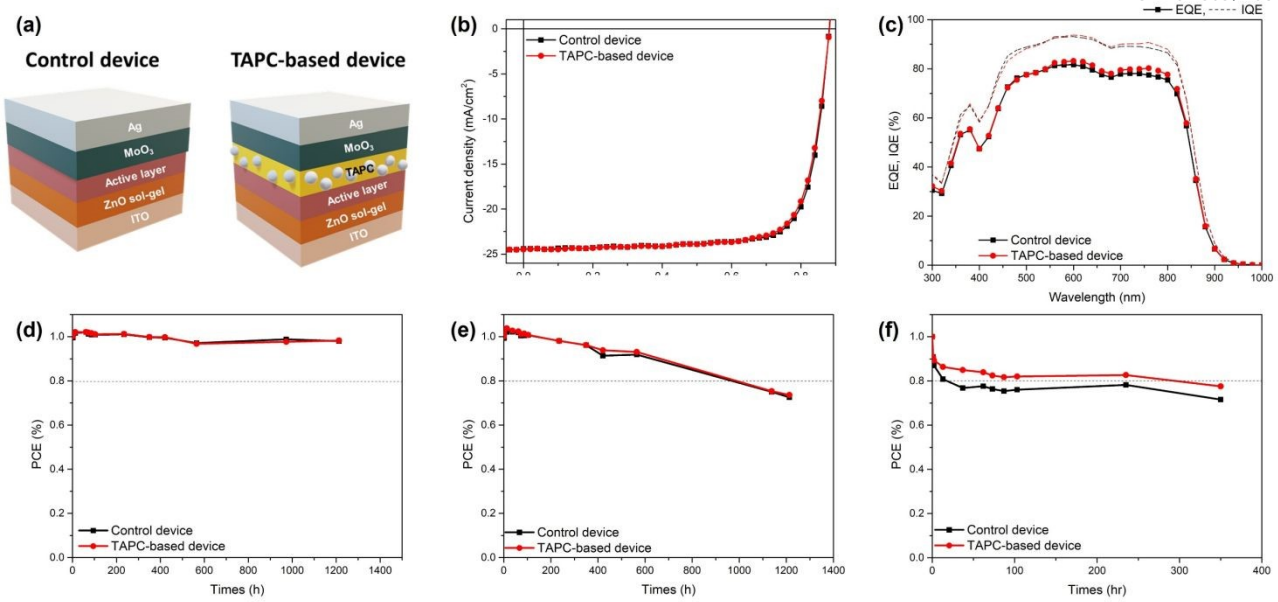

Fig. 2 (a) Device architecture of OSCs (ITO/ZnO/PM6:L8-BO/HTL/Ag) with different HTL: a single-layer MoO_3 for the control device and MoO_3/TAPC hybrid HTL for the TAPC-based device (b) Current density–voltage (*J–V*) and (c) EQE and IQE curves of the optimized devices with single-layer MoO_3 device and MoO_3/TAPC hybrid HTL device under illumination of AM 1.5G 1-sun (100 mW cm^{-2}). Photovoltaic parameter of single-layer MoO_3 and MoO_3/TAPC hybrid HTL devices under different aging conditions: (a) storage, (b) thermal stress (60 °C), and (c) light stability. All tests were conducted on unit cell devices.

Table 1 Photovoltaic parameters of the optimized MoO_3/TAPC hybrid HTL OSCs under AM 1.5G illumination, 100mW cm^{-2}.

Structure	J_{SC} [mA cm^{-2}]	J_{cal} [a] [mA cm^{-2}]	V_{OC} [V]	FF [%]	PCE [%]
single-layer MoO_3 device	24.33	23.40	0.880	76.58	16.39 (16.34 ± 0.15)
MoO_3/TAPC hybrid HTL device	24.48	23.78	0.882	76.35	16.49 (16.44 ± 0.03)

[a] J_{cal} values were obtained from the EQE curves.

In the following experiments, the correlation between TAPC concentration and device performance was systematically investigated while maintaining the MoO_3 layer thickness at fixed values ranging from 0 to 10 nm (Fig. S3–S6, Table S2–S5). Specifically, for the device without MoO_3 (0 nm), the introduction of 0.5 mg/mL TAPC led to increase in both J_{SC} (from 20.55 to 20.94 mA/cm^{-2}) and V_{OC} (from 0.132 to 0.153V). A similar enhancement was observed at a MoO_3, thickness of 5 nm, where the MoO_3/TAPC hybrid HTL outperforming the single-layer MoO_3 reference, reaching a J_{SC} of 23.69 mA/cm^{-2} and V_{OC}=0.875V. Likewise, for the 10 nm condition, the MoO_3/TAPC hybrid bilayer showed a significant upward trend, with J_{SC} rising from 21.66 to 22.34 mA/cm^{-2} and V_{OC} increasing from 0.810 to 0.831 V. Interestingly, in contrast to the optimized 2.5 nm condition, the efficiency for the 0, 5, and 10 nm MoO_3 layers exhibited a positive correlation with increasing TAPC concentration. Especially, This behavior is attributed to the ability of TAPC to compensate for the intrinsic electrical limitations of thicker MoO_3 layers, which typically suffer from low conductivity and high series resistance.[25] The increased amount of TAPC facilitates charge transfer at the interface, effectively inducing p-doping and enhancing the conductivity.[19]

Based on optimal MoO_3 thickness of 2.5 nm, we subsequently optimized the TAPC layer (Fig. S4a and Table S3). Furthermore, with the MoO_3. layer thickness maintained at 2.5 nm, the corresponding TAPC film thicknesses were determined via α-step measurements to be 28.50, 29.30, and 36.90 nm, depending on the concentration. Among these, the 28.50 nm-thick TAPC layer proved to be optimal, exhibiting the highest efficiency of 16.49% PCE for the MoO_3/TAPC layer. This optimization resulted in improved photovoltaic parameters (J_{SC} =24.48 mA/cm^{-2} and V_{OC}=0.882V) compare to the single-layer MoO_3(J_{SC} =24.33 mA/cm^{-2} and V_{OC}=0.880 V). To ensure the reproducibility of these results, Fig. S4b presents the average performance statistics from five independent devices. As illustrated in the *J-V* curve in Fig. 2b, while both the single-layer MoO_3 (black line) or a MoO_3/TAPC hybrid HTL (red line) exhibited comparable PCEs, the hybrid strategy facilitated a simultaneous enhancement in both J_{SC} and V_{OC} (Table 2). In addition, this tendency was consistently reflected in the external quantum efficiency (EQE) spectrum presented in Fig. 2c, where J_{cal} showed a deviation of less than 5%.[26] To resolve the optical and electrical effects, we analyzed the Internal Quantum Efficiency (IQE). In both EQE and IQE analysis, the

Published on 05 February 2026. Downloaded on 2/27/2026 1:10:22 AM.
Sustainable Energy & Fuels Accepted Manuscript

View Article Online DOI: 10.1039/D5SE01715A

Published on 05 February 2026. Downloaded on 2/27/2026 1:10:22 AM.

Sustainable Energy & Fuels Accepted Manuscript

spectral response exhibited a marked increase across the broad wavelength range of 550–850 nm. The uniform enhancement in IQE demonstrates that the improved performance is primarily attributed to an increase in the internal photon-to-electron conversion efficiency.[18] This suggests that the MoO_3/TAPC interface is electrically superior, facilitating the efficient collection of photogenerated charges.[10] To provide a more in-depth analysis, the EQE was investigated as a function of TAPC concentration at a fixed MoO_3 thickness of 10 nm (Fig. S6b). Consequently, the EQE values were broadly improved in the 500–850 nm region with higher concentrations, matching the J_{SC} recorded in the *J-V* curves. Furthermore, the J_{cal} values exhibited an increase from 20.99 mA/cm^{-2} for the single-layer MoO_3 to 21.77 mA/cm^{-2}at a TAPC concentration of 0.5 mg/mL. In particular, the J_{cal} was further enhanced to 22.34 mA/cm^{-2} at a TAPC concentration of 2 mg/mL. These results align with the increasing trend of J_{SC} observed previously and are intimately linked to the enhancement in EQE. To further elucidate these findings, additional UV-Vis spectra were analyzed. Consequently, the optical signals strengthened broadly across the visible region with increasing TAPC content, as illustrated in Fig. S6c. The TAPC-induced light scattering accounts for this optical gain, resulting in enhanced optical utilization and boosted photon harvesting within the active layer. [27,28] Consequently, this high efficiency effectively suppresses recombination, enhances charge transport, and will be presented in detail in the following section. In Fig. S7, a schematic energy-level diagram is provided, illustrating the HOMO and LUMO levels of the respective materials. TAPC, with a HOMO level of 5.25 eV (yellow), was well aligned in energy between the HOMO of the active layer (brick red) and the work function of MoO_3 (green, 5.20 eV). This energy cascade is consistent with prior reports, indicating its role in promoting efficient hole transport while mitigating interfacial energy barriers.[18,29] The long-term stability of devices incorporating TAPC is presented in Fig. 2d–f. Fig. 2d and 2e present the evolution of PCE under dark storage conditions. Notably, for the storage stability test shown in Fig. 2d at 25 °C, the devices were encapsulated with a non-conductive adhesive (NCA). In contrast, Fig. 2e displays the degradation behavior under thermal stress at 60 °C for 1213 h. In contrast, Fig.2f illustrates the photostability, where the PCE was monitored under continuous 1-sun illumination at 25 °C for 374 h. Under the dark state, the device exhibited no discernible change in PCE with the temperature variation from 25 °C to 60 °C. Nevertheless, upon continuous exposure to 1 sun illumination, the PCE dropped to 95% of its initial value within 2 h and subsequently stabilized at 78% and 72% after 374 h, respectively. These results demonstrate that the MoO_3/TAPC hybrid HTL effectively mitigates photo-induced degradation. These findings are consistent with previous reports on small-molecule-based bilayer architectures such as ITO+MoO_3/SAM[7] or TCTA/MoO_3[15] structures, underscoring the potential of MoO_3/TAPC hybrids for enhancing the operational stability of OSCs.[26,30,31] The overall X-ray photoelectron spectroscopy (XPS) survey spectra are presented in Fig. S8. The characteristic peaks for O 1s, Mo 3d, and N 1s were identified at 530, 231, and 398 eV, respectively. Overall, all characteristic peaks in the MoO_3/TAPC hybrid HTL film shifted toward lower binding energy. As shown in Fig. 3a, the fitted Mo 3d XPS spectra confirms the presence of dual oxidation states, specifically Mo^{5+} and Mo^{6+}. The Mo^{5+} peaks were observed at 231.38 eV for the single-layer MoO_3. film and 231.05 eV for the MoO_3/TAPC hybrid HTL film. Likewise, the Mo^{6+} binding energy shifted toward a lower value by 0.3 eV, decreasing from 232.48 eV in the single-layer MoO_3 to 232.19 eV in the MoO_3/TAPC hybrid HTL. The atomic concentration ratio of Mo^{5+}/(Mo^{6+}+Mo^{5+}) exhibited an increase from 6.71% to 8.28% upon the incorporation of TAPC. This indicates the chemical reduction of MoO_3 induced by TAPC, which can lead to enhanced charge transfer through the interfacial charge distribution.[15,32] To further elucidate the underlying cause, we also investigated the electronic environment of the TAPC layer by analyzing the evolution of the N 1s (Fig. 3b). consistent with the aforementioned results, the N^+ peaks for the single-layer MoO_3 film and the MoO_3/TAPC hybrid HTL film were identified at 401.51 eV and 401.08 eV, respectively. Similarly, the C–N peaks shifted from 398.1 eV to 397.83 eV, following the same downward trend observed in the Mo 3d. The universal shift toward lower binding energies observed in the XPS survey, Mo 3d, and N 1s indicates that the interfacial charge transfer at the MoO_3/TAPC interface effectively optimizes carrier transport, thereby facilitating efficient charge extraction from the active layer. [33,34] This observation aligns well with the interfacial band bending with Fig. S7, confirming the formation of a favorable hole extraction of TAPC. Fig. 3c displays the PL spectra (600–800 nm) of the device fabricated with an ITO/active layer/HTL architecture, under excitation at 580 nm. The PL of the MoO_3/TAPC hybrid HTL film (red line) is strongly quenched relative to that of the single-layer MoO_3 film (black line) at the 760 nm peak. This suggests that, serving as a charge carrier, the hybrid HTL with MoO_3/TAPC enables more effective charge transport than the device employing single-layer MoO_3.[24,35,36] The complementary function of TAPC was additionally substantiated by recombination analysis. The *J–V* characteristics were measured under various light intensities (P_{light}) to evaluate the recombination dynamics of the single-layer MoO_3 and the MoO_3/TAPC hybrid HTL OSCs.

$$J_{SC} \propto P^{\alpha}_{light}$$

Where α is an exponential factor derived from the slope of the J_{SC}–P_{light} curve, and a value of α approaching unity indicates a more effective suppression of bimolecular recombination in OSCs.[37] As shown in Fig. 3d, the α values of the single-layer MoO_3 and MoO_3/TAPC hybrid HTL devices are 1.032 and 1.022, respectively, indicating that bimolecular recombination is more effectively suppressed in the MoO_3/TAPC hybrid HTL. This implies that TAPC offers a complementary charge transport pathway, leading to improved charge extraction efficiency beyond what can be attained with a single-layer MoO_3.[18] Furthermore, the correlation between V_{OC} and P_{light} was systematically examined to elucidate the trap-assisted recombination mechanism in OSCs.

$$V_{OC} \propto n(kT/q)\ln(P_{light})$$

View Article Online
DOI: 10.1039/D5SE01315A

Where *k*, *T*, and *q* denote the Boltzmann constant, the absolute temperature, and the elementary charge, respectively.[2] The slope of *n* typically falls within the range of 1–2, and values approaching unity indicate a reduction in the interfacial charge trap density. Fig. 3e reveals that the control device exhibited an *n* value of 1.064, while the MoO_3/TAPC hybrid HTL device demonstrated a marginally reduced value of 1.061. This suggests that trap-assisted recombination is suppressed in MoO_3/TAPC hybrid HTL devices and that incorporating a TAPC interlayer can effectively reduce interfacial defects with the active layer.[38] In addition, Fig. 3f presents the dark current density–voltage (J_D–V) characteristics measured within the range of –0.5 to 0.5 V to evaluate the leakage current of the fabricated device. Consequently, the MoO_3/TAPC hybrid HTL devices demonstrated a significant suppression of leakage current, accompanied by an enhancement in diode characteristics. Collectively, TAPC serves a complementary functional role by simultaneously enhancing light extraction efficiency, facilitating charge transport, and suppressing recombination, thereby synergistically complementing MoO_3 and contributing to the improvement of the device J_{SC}.[39]

Fig. 3g shows the evaluation of hole mobility in the device configured with an ITO/PEDOT:PSS/active layer/HTL/Ag architecture. The hole mobilities of the single-layer MoO_3 device (black) and the MoO_3/TAPC hybrid HTL (red) device were determined to be 1.102×10^{-4} cm^2 V^{-1}s^{-1} and 1.195×10^{-4} cm^2 V^{-1}s^{-1}, respectively. The MoO_3/TAPC hybrid HTL device exhibited a slightly enhanced hole mobility trend, which could exert a significant influence on the charge-transport pathways.[23]

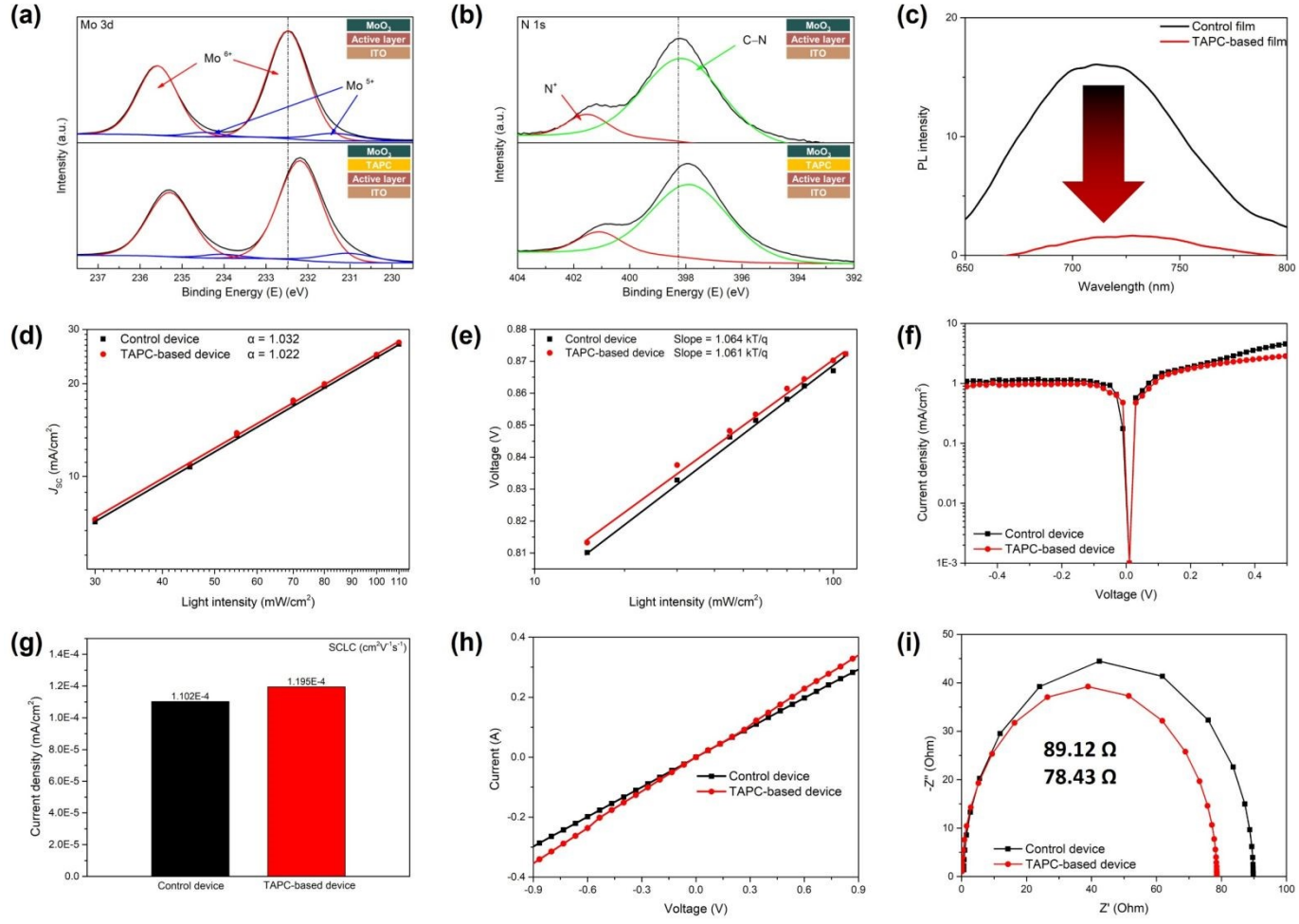

Fig. 3 (a) N 1s and (b) Mo 3d XPS spectra of ITO/BHJ/MoO_3 and ITO/BHJ/TAPC/MoO_3 films. (c) PL intensity, Dependence of (d) J_{SC} and (e) V_{OC} on light intensity. (f) Dark current density (J_D)–voltage(V) characteristics, (g) hole mobility determined by the SCLC method, (h) I–V curves and (i) Nyquist plots for the single-layer MoO_3 and MoO_3/TAPC hybrid HTL OSCs.

Moreover, this result is consistent with the trend observed in the preceding PL data, which showed significantly stronger quenching.[11] Additionally, the charge transport characteristics of the two devices are presented in Fig. 3h, exhibiting relatively high conductivities of 1.616 × ×10^{-6} S cm^{-1} and 1.624×10^{-6} S cm^{-1}, respectively. In addition, Fig. 3i presents the results of interfacial resistance analysis obtained through electrochemical impedance spectroscopy (EIS). These values were also measured to be 89.12 Ω and 78.43 Ω, respectively. The reduced resistance suggests that the hybrid structure within the MoO_3/TAPC can suppress interfacial recombination while facilitating efficient exciton dissociation.[37,40] Accordingly, the incorporation of TAPC as an additional interlayer between the active layer and MoO_3 was found to enable efficient charge

Published on 05 February 2026. Downloaded on 2/27/2026 1:10:22 AM.

Sustainable Energy & Fuels Accepted Manuscript

View Article Online
DOI: 10.1039/D5SE01715A

transfer across the interface.[6,39] Fig. 4 depicts the AFM topographies (a–b: pristine MoO_3, d–e: MoO_3/TAPC) together with the corresponding contact angle measurements for the HTLs incorporated into the ITO/ZnO/Active layer/HTLs configuration. As shown in Fig. 4d, the MoO_3/TAPC hybrid HTL surface film demonstrated an RMS roughness of 0.736 nm, representing a reduction of 1.049 nm compared to the single-layer MoO_3 film (Fig. 4a). Examination of the 3D surface morphology reveals that the MoO_3/TAPC hybrid HTL surface (Fig. 4e) exhibits a more refined and three-dimensional configuration, indicating enhanced surface texturing. Fig. 4c and 4f depict the contact angle measurement results acquired under the same experimental conditions. The MoO_3/TAPC hybrid HTL film exhibited a water contact angle of 91.84°, in contrast to the markedly higher value of 101.01° observed for the single MoO_3 film. Meanwhile, the DIM contact angle was measured to be 36.60° for the MoO_3/TAPC hybrid HTL film, in contrast to 36.22° observed for the pristine MoO_3 film. Utilizing the acquired data, the surface energy estimated via the Wu model[2] was determined to be 41.92 mN m^{-1} for the MoO_3/TAPC hybrid HTL film, representing an increase relative to that of the single MoO_3 film (37.14 mN m^{-1}). This suggests that TAPC can enhance interfacial adhesion, thereby facilitating the formation of a more stable interface.[41] To validate the mini-modules based on the MoO_3/TAPC hybrid bilayer structure, we systematically evaluated device performance across different active areas, ranging from unit cells (0.04 cm^2) to single large-area cells (1.00 cm^2) and mini-modules (4.725 cm^2).[1,2] Detailed photovoltaic parameters for the 1.00 cm^2 devices are provided in Table S6.

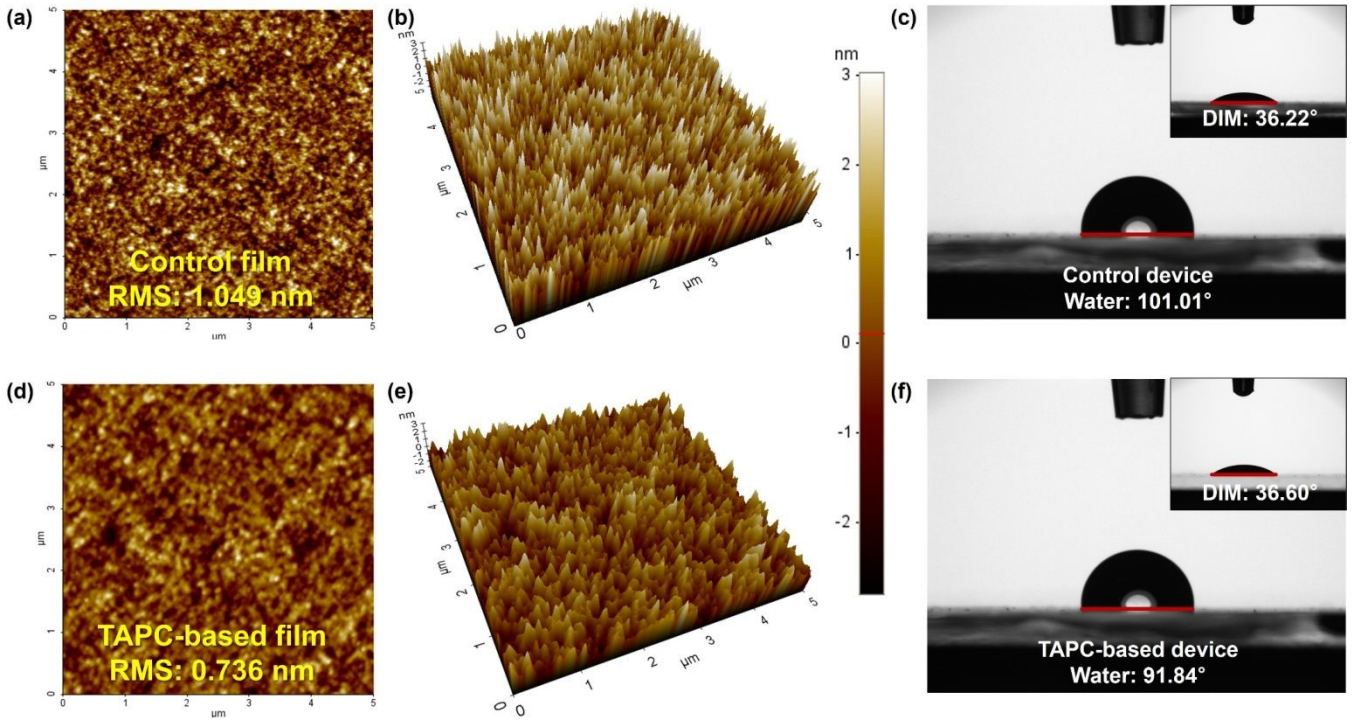

Fig. 4 (a,d) AFM height and (b,e) 3D topography images with the configuration of ITO/ZnO/active layer/MoO_3 in single-layer MoO_3 film and ITO/ZnO/active layer/TAPC/MoO_3 in MoO_3/TAPC hybrid HTL film. (c,f) Contact angle of single-layer MoO_3 film and MoO_3/TAPC hybrid HTL films with the configuration of ITO/active layer/MoO_3 and ITO/active layer/ TAPC/MoO_3.

The cell of 1.00 cm^2 with MoO_3/TAPC hybrid HTL devices demonstrably displayed an improvement from 10.48% to 11.15% compared with the single-layer MoO_3-based OSCs. The result demonstrates that MoO_3/TAPC hybrid HTL OSCs consistently exhibited superior performance compared to the single-layer MoO_3-based devices. Building upon these scalable properties, Fig. 5a presents a schematic representation of the inverted-architecture OSC module with an active area of 4.725 cm^2.The upper schematic illustration presents a single-layer MoO_3 HTL, while the lower schematic illustration depicts a module incorporating MoO_3/TAPC hybrid HTL, both identically configured with a three-cell series connection. On the left side of each schematic, a simplified diagram of the module fabrication process is presented, indicating the scribing lines. In the module, P1 corresponds to the scribing line that partitions the ITO film to define the sub-cells, P2 designates the region where the ETL and active layer are removed, and finally, P3 represents the section where the HTL and Ag are ablated to delineate the active area. The *J–V* curve of the MoO_3/TAPC hybrid HTL module is presented in Fig. 5b, and the corresponding data are summarized in Table 2, together with a photograph of the fabricated device with an active area of 4.725 cm^2. In particular, the MoO_3/TAPC hybrid HTL module exhibited an improvement in both J_{SC} and PCE from 13.46% to 13.95% compared with the single-layer MoO_3-based module, which is consistent with the trend observed in the unit cells.

Published on 05 February 2026. Downloaded on 2/27/2026 1:10:22 AM.

Sustainable Energy & Fuels Accepted Manuscript

Please do not adjust margins

View Article Online
DOI: 10.1039/D5SE01315A

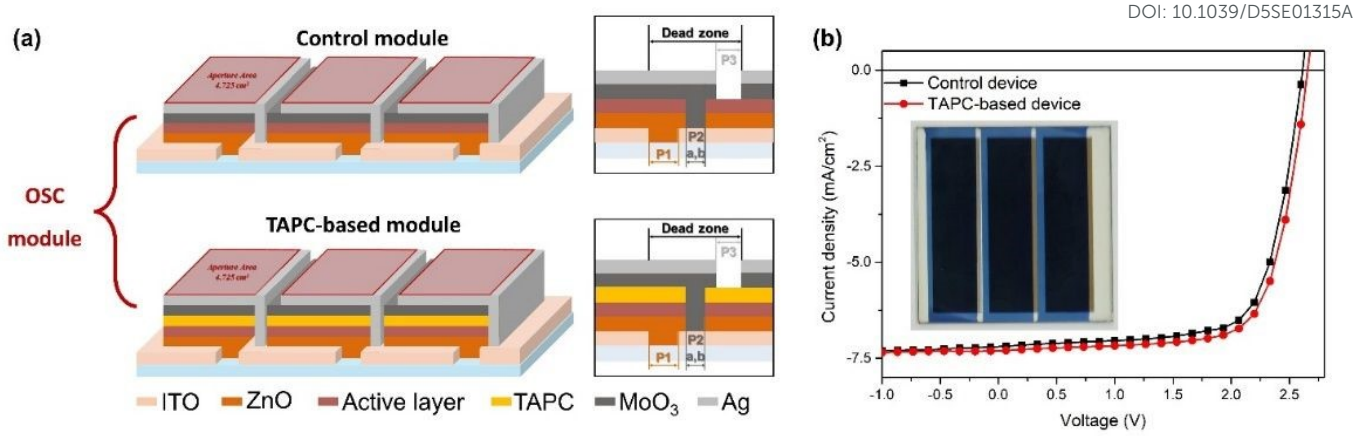

Fig. 5 (a) Schematic images of fabricated mini-modules (active area of 4.725 cm^2 with 3-cell). (b) Current density–voltage (*J*–*V*) of the optimized devices with single-layer MoO_3 and MoO_3/TAPC hybrid HTL device with photographs of module.

Table 2 Photovoltaic parameters of the optimized the single-layer MoO_3 device and MoO_3/TAPC hybrid HTL OSCs under AM 1.5G illumination, 100mW cm^{-2}.

Structure	J_{SC} [mA cm^{-2}]	V_{OC} [V]	FF [%]	PCE [%]
Single-layer MoO_3 device	7.20	2.613	71.57	13.46 (13.84 ± 0.08)
MoO_3/TAPC hybrid HTL device	7.30	2.657	71.87	13.95 (13.43 ± 0.15)

Although the absolute PCE of the 1.00 cm^2 single cell was slightly lower than that of the mini-module, this result indicates that the TAPC layer effectively mitigates the performance deviation caused by area enlargement, likely by improving the interfacial contact and alleviating the charge-extraction constraints at the MoO_3 interface. Thus, these results provide compelling evidence that the TAPC-based hybrid HTL constitutes a scalable approach, exhibiting high versatility and practicality as an HTL material suitable for diverse organic optoelectronic devices as well as module systems.[16]

Conclusions

In this study, we developed a MoO_3/TAPC hybrid bilayer HTL by integrating the superior interfacial properties of TAPC with the robust hole-transporting capabilities of MoO_3. When integrated into inverted OSCs, the MoO_3/TAPC hybrid bilayer yielded a PCE of 16.49% in unit cells. This performance enhancement stems from a synergistic interaction between TAPC and MoO_3, which induces chemical reduction and optimizes charge carrier dynamics. Furthermore, the hybrid layer simultaneously suppresses interfacial recombination and facilitates efficient charge transport through light-scattering effects, thereby promoting broadband photon harvesting. To further demonstrate practical applicability, a mini-module with an active area of 4.725 cm^2 achieved a PCE of 13.95%, with enhanced J_{SC} contributing significantly to the performance improvement. Furthermore, this stable interfacial interaction significantly contributes to long-term stability Collectively, these results demonstrate a promising strategy for developing stable and scalable OSCs toward future commercialization.

Conflicts of interest

There are no conflicts to declare.

Acknowledgements

This study was supported by the Material Components Technology Development Program (20019197) by the Ministry of Trade, Industry and Energy (MOTIE), Republic of Korea. This work was also partially supported by the Human Resources Development Program of the Korea Institute of Energy Technology Evaluation and Planning (KETEP), funded by the Ministry of Trade, Industry and Energy, Republic of Korea (No. RS-2023-00237035).

Notes and references

1 S. Yang, X. Huang, Y. Cho, S. Koo, Y. Ouyang, Z. Sun, S. Jeong, T. L. H. Mai, W. Kim, L. Zhong, S. Chen, C. Zhang, H. Lee, S. Yoon, L. Chen and C. Yang, *Angewandte Chemie International Edition*, 2025, e202424287.

Published on 05 February 2026. Downloaded on 2/27/2026 1:10:22 AM.
Sustainable Energy & Fuels Accepted Manuscript

Please do not adjust margins

View Article Online
DOI: 10.1039/D5SE01315A

2 Y. C. Kim, S. J. Jeon, N. G. Yang, J. Y. Kim, Y. W. Han and D. K. Moon, *ACS Appl Mater Interfaces*, 2025, 17, 6626–6638.

3 S. J. Jeon, Y. C. Kim, J. Y. Kim, J. H. Kim, N. G. Yang, Y. J. Lee, H. S. Lee, Y. H. Kim, G. W. Kim, E. M. Jang, B. Lee, C. Yang and D. K. Moon, *Chemical Engineering Journal*, 2023, 472, 144850.

4 A. Liang, Y. Sun, S. Chung, J. Shin, K. Sun, C. Zhu, J. Zhao, Z. Zhao, Y. Zhong, G. Zhang, K. Cho and Z. Kan, *Nanomicro Lett*, 2025, 17, 72.

5 J. Yuan, Y. Zhang, L. Zhou, G. Zhang, H. L. Yip, T. K. Lau, X. Lu, C. Zhu, H. Peng, P. A. Johnson, M. Leclerc, Y. Cao, J. Ulanski, Y. Li and Y. Zou, *Joule*, 2019, 3, 1140–1151.

6 X. Dai, B. Fan, W. Zhou, Y. Li, X. Xu and Q. Peng, *ACS Energy Lett*, 2025, 10, 2045–2051.

7 X. Xiong, B. Hu, S. Tai, G. Lu, H. Fu and Q. Zheng, *Adv Funct Mater*, 2025, 2505515.

8 W. Wang, Z. Lin, X. Li, C. Zhang, T. Yang and Y. Liang, *ACS Appl Mater Interfaces*, 2022, 14, 18736–18743.

9 B. Zhao, X. Huang, S. Chung, M. Zhang, Y. Zhong, A. Liang, Z. Zhao, C. Zhu, J. Zhao, S. Kim, J. Kim, M. Wang, S. Chen, K. Cho, Y. Wang and Z. Kan, *eScience*, 2025, 5, 100305.

10 A. Panagiotopoulos, G. Kakavelakis, K. Almpanidis, L. Askew, D. I. Kutsarov and S. R. P. Silva, *J Mater Chem A Mater*, 2025, 13, 8774–8789.

11 L. Caliò, B. R. Patil, J. Benduhn, K. Vandewal, H. G. Rubahn, M. Madsen, S. Kazim and S. Ahmad, *Sustain Energy Fuels*, 2018, 2, 2296–2302.

12 Y. Gong, Y. Dong, B. Zhao, R. Yu, S. Hu and Z. Tan, *J Mater Chem A Mater*, 2020, 8, 978–1009.

13 Q. Huang, J. Jing, K. Zhang, Y. Chen, A. Song, Z. Liu and F. Huang, *J Mater Chem A Mater*, 2022, 10, 23973–23981.

14 C. Song, X. Huang, T. Zhan, L. Ding, Y. Li, X. Xue, X. Lin, H. Peng, P. Cai, C. Duan and J. Chen, *ACS Appl Mater Interfaces*, 2022, 14, 40851–40861.

15 Q. Xi, J. Qin, O. J. Sandberg, N. Wu, R. Huang, Y. Li, M. Saladina, C. Deibel, R. Österbacka and C.-Q. Ma, *ACS Appl Mater Interfaces*, 2025, 17, 15456–15467.

16 Y. W. Han, H. S. Lee and D. K. Moon, *ACS Appl Mater Interfaces*, 2021, 13, 19085–19098.

17 H.-C. Yeh, H.-F. Meng, H.-W. Lin, T.-C. Chao, M.-R. Tseng and H.-W. Zan, *Org Electron*, 2012, 13, 914–918.

18 H. Tang, J. Wu, H. Liu, B. Wang, H. Wang, Y. Li, Y. Fu and Z. Xie, *Org Electron*, 2021, 93, 106140.

19 H. Shekhar and N. Tessler, *Sustain Energy Fuels*, 2020, 4, 5618–5627.

20 L. Yang, F. Cai, Y. Yan, J. Li, D. Liu, A. J. Pearson and T. Wang, *Adv Funct Mater*, 2017, 27, 1702613.

21 M. Yan, P. J. Skabara and H. Meng, *J Mater Chem C Mater*, 2023, 11, 8480–8485.

22 W. B. Tarique, M. H. Rahaman, S. S. Dipta, A. H. Howlader and A. Uddin, *Nanomanufacturing*, 2024, 4, 81–98.

23 J. Wang, K. Liu, L. Ma and X. Zhan, *Chem Rev*, 2016, 116, 14675–14725.

24 X. Sun, J. Lv, X. Ding, C. Gao, G. Zhang, J. Zeng, C. Zou, W. Liu, S. Zhao, X. Ouyang, C. Yang, H. Hu and H. Chen, *ACS Mater Lett*, 2024, 6, 3282–3290.

25 S. Chambon, L. Derue, M. Lahaye, B. Pavageau, L. Hirsch and G. Wantz, *Materials*, 2012, 5, 2521–2536.

Published on 05 February 2026. Downloaded on 2/27/2026 1:10:22 AM.

Sustainable Energy & Fuels Accepted Manuscript

Please do not adjust margins

26 W. B. Tarique, A. H. Howlader, S. S. Dipta, A. Pratik and A. Uddin, *Sustain Energy Fuels*, 2025, 9, 2109–2118.

27 S. Ju, H. Kim, H. Kwak, C. Kang, I. Jung, S. Oh, S. G. Lee, J. Kim, H. J. Park and K. T. Lee, *Sci Rep*, 2023, 13, 20649.

28 M. Sandzhieva, D. Khmelevskaia, D. Tatarinov, L. Logunov, K. Samusev, A. Kuchmizhak and S. V. Makarov, *Nanomaterials*, 2022, 12, 3916.

29 J. Zhang, L. Zhang and J. Chen, *ACS Appl Polym Mater*, 2024, 6, 7742–7750.

30 L. Duan, H. Yi, Y. Zhang, F. Haque, C. Xu and A. Uddin, *Sustain Energy Fuels*, 2019, 3, 723–735.

31 A. Takahara, M. Nakano, M. Shahiduzzaman, M. Karakawa, T. Taima, K. Takahashi, H. Shibata and A. Masuda, *Sustain Energy Fuels*, 2021, 5, 3092–3096.

32 C. C. Lee, S. Biring, S. J. Ren, Y. Z. Li, M. Z. Li, N. R. Al Amin and S. W. Liu, *Org Electron*, 2019, 65, 150–155.

33 X. Zhu and W. Wan, *J Alloys Compd*, 2025, 1039, 183126.

34 J. Zhang, Y. Sun, C. Huang, B. Yu and H. Yu, *Adv Energy Mater*, 2022, 12, 2202542.

35 S. Huang, Y. Tang, Y. Dang, X. Xu, Q. Dong, B. Kang and S. R. P. P. Silva, *ACS Sustain Chem Eng*, 2018, 6, 6702–6710.

36 B. Deng, H. Lian, B. Xue, R. Song, S. Chen, Z. Wang, T. Xu, H. Dong and S. Wang, *Small*, 2023, 19, 2207505.

37 J. Wang, D. Zhou, J. Quan, S. Lan, F. Wang, L. Hu, W. Wan, Y. Tong, B. Hu, R. Lv, H. Xu, Z. Li and L. Chen, *ACS Sustain Chem Eng*, 2024, 12, 11385–11395.

38 C. Liu, Y. Lian, J. Song, J. Liu, Z. Bi, W. Ma and Y. Sun, *Adv Funct Mater*, 2025, 35, 2417786.

39 H. Li, J. Tan, S. Yang, Y. Sun and H. Yu, *ACS Appl Mater Interfaces*, 2024, 16, 20443–20453.

40 Y. Wang, K. Sun, C. Li, C. Zhao, C. Gao, L. Zhu, Q. Bai, C. Xie, P. You, J. Lv, X. Sun, H. Hu, Z. Wang, H. Hu, Z. Tang, B. He, M. Qiu, S. Li and G. Zhang, *Advanced Materials*, 2024, 36, 2411957.

41 F. Jin, R. Peng, Y. Qiu, J. Zhang and Z. Ge, *ACS Appl Energy Mater*, 2023, 6, 9532–9542.

View Article Online
DOI: 10.1039/D5SE01315A

Published on 05 February 2026. Downloaded on 2/27/2026 1:10:22 AM.

Sustainable Energy & Fuels Accepted Manuscript

View Article Online
DOI: 10.1039/D5SE01315A

Data Availability Statement:

All data that support the findings of this study are contained within the article and its ESI.

Published on 05 February 2026. Downloaded on 2/27/2026 1:10:22 AM.

Sustainable Energy & Fuels Accepted Manuscript